Journal of Hydrology (2008) **356**, 327–343

available at www.sciencedirect.com

ScienceDirect

journal homepage: www.elsevier.com/locate/jhydrol

Ground surface temperature simulation for different land covers

William R. Herb *, Ben Janke, Omid Mohseni, Heinz G. Stefan

University of Minnesota, Department of Civil Engineering, St. Anthony Falls Laboratory, 2—3rd Avenue SE, Minneapolis, MN 55414, United States

Received 23 August 2007; received in revised form 11 April 2008; accepted 25 April 2008

KEYWORDS
Heat transfer;
Land use;
Pavement;
Vegetation;
Temperature;
Thermal pollution

Summary A model for predicting temperature time series for dry and wet land surfaces is described, as part of a larger project to assess the impact of urban development on the temperature of surface runoff and coldwater streams. Surface heat transfer processes on impervious and pervious land surfaces were investigated for both dry and wet weather periods. The surface heat transfer equations were combined with a numerical approximation of the 1-D unsteady heat diffusion equation to calculate pavement and soil temperature profiles to a depth of 10 m. Equations to predict the magnitude of the radiative, convective, conductive and evaporative heat fluxes at a dry or wet surface, using standard climate data as input, were developed. A model for the effect of plant canopies on surface heat transfer was included for vegetated land surfaces. Given suitable climate data, the model can simulate the land surface and sub-surface temperatures continuously throughout a six month time period or for a single rainfall event.

Land surface temperatures have been successfully simulated for pavements, bare soil, short and tall grass, a forest, and two agricultural crops (corn and soybeans). The simulations were run for three different locations in US, and different years as imposed by the availability of measured soil temperature and climate data. To clarify the effect of land use on surface temperatures, the calibrated coefficients for each land use and the same soil coefficients were used to simulate surface temperatures for a six year climate data set from Albertville, MN. Asphalt and concrete give the highest surface temperatures, as expected, while vegetated surfaces gave the lowest. Bare soil gives surface temperatures that lie between those for pavements and plant-covered surfaces. The soil temperature model predicts hourly surface temperatures of bare soil and pavement with root—mean—square errors (RMSEs) of 1—2 °C, and hourly surface temperatures of vegetation-covered surfaces with RMSEs of 1—3 °C.

* Corresponding author. Tel.: +1 612 624 4629; fax: +1 612 624 4398.
E-mail addresses: wrherb@comcast.net (W.R. Herb), janke024@umn.edu (B. Janke), omohseni@umn.edu (O. Mohseni), stefa001@umn.edu (H.G. Stefan).

0022-1694/$ - see front matter
doi:10.1016/j.jhydrol.2008.04.020

Nomenclature

α_s	surface albedo (dimensionless)
β	thickness ratio for surface runoff conduction
ε	surface emissivity (dimensionless)
θ	soil moisture content (dimensionless)
θ_v	virtual air temperature (°C)
ρ	density (kg/m^3)
σ	Stefan–Boltzmann constant (kJ/K^4/m^2/day)
C_e	soil evaporation parameter (dimensionless)
C_{fc}	forced convection bulk transfer coefficient (dimensionless)
C_{nc}	free convection bulk transfer coefficient (dimensionless)
CH_f	foliage aerodynamic roughness (m)
C_f	foliage bulk transfer coefficient (m)
CS_h	wind sheltering coefficient (dimensionless)
C_p	specific heat (J/kg/K)
CR	cloudiness factor (0–1, dimensionless)
δ	conduction layer thickness (m)
δz	node spacing (m)
Δt	analysis time step (s)
Δz	discrete model layer thickness (m)
D	thermal diffusivity (m^2/s)
e_a	atmospheric water vapor pressure (Pa)
e_s	saturation vapor pressure at surface temperature (Pa)
h_{li}	incoming longwave radiation (W/m^2)
h_{lo}	outgoing longwave radiation (W/m^2)
h_s	net solar radiation (W/m^2)
h_{conv}	convection between land or water surface and atmosphere (W/m^2)
h_{evap}	evaporative heat transfer rate (W/m^2)
h_{net}	net (total) heat transfer at surface (W/m^2)
h_{rad}	net shortwave and longwave radiation (W/m^2)
h_{ro}	surface runoff heat transfer rate (W/m^2)
i	precipitation rate (m/s); also vertical distance indice
j	time indice
L_v	latent heat of vaporization of water (J/kg)
v	vegetation density (0–1, dimensionless)
p	atmospheric pressure (Pa)
P	precipitation depth (m)
q	specific humidity (kg$_w$/kg$_a$)
r_a	aerodynamic resistance (s/m)
r_s	stomatal resistance (s/m)
R_s	observed solar radiation (W/m^2)
RMSE	root mean square error
t	time (s)
T_a	air temperature (°C)
T_{dp}	dewpoint temperature (°C)
T_f	average foliage temperature (°C)
T_s	surface temperature (°C)
u	wind speed (m/s)
z	depth coordinate (m)

Introduction

Land use change has a number of effects on the hydrology of a watershed. Increased impervious surface area can lead to reduced infiltration and increased surface runoff during rainfall events. Erosion, sediment and pollutant transport processes due to this surface runoff have been the subject of many experimental and modeling studies (e.g. Kleinman et al., 2006; Emmerich et al., 1989).

A less studied aspect of surface runoff is the heat transport associated with it, and the effect of this heat transport on aquatic habitat. Several studies have examined heat loading of water bodies by surface runoff from pavement (Van Buren et al., 2000; Ul Haq and James, 2002; Roa-Espinosa et al., 2003), and have highlighted the importance of ground surface temperature in controlling thermal loading.

The ground temperature model described in this paper was developed as a first step to estimate the heat loading of surface runoff to receiving water bodies, e.g. coldwater streams. Dry weather ground temperatures represent an initial condition for rainfall events, and control the amount of heat energy available to create a temperature change in the surface runoff. Air temperature, solar radiation, and cloud cover conditions can change rapidly prior to the onset of rainfall, so that relatively high temporal resolution is required to capture the heat transfer dynamics during the initial phases of a rainfall event.

Ground surface temperature is a parameter of interest in a variety of hydrological studies. Surface temperature and the associated flux of water vapor are important boundary conditions for atmospheric models (Best et al., 2005; Mengelkamp et al., 1999). Remote sensing is increasingly being used to study relationships between ground surface temperature, vegetative cover, and water fluxes and to study relationships between ground surface temperatures and global climate change (e.g. Dang et al., 2007). Vegetation and ground surface temperature are also studied in the context of crop modeling (Luo et al., 1992; Mihailovic and Eitzinger, 2007).

Temperature models for paved surfaces have been developed to better understand pavement durability and to enable better tuning of pavement properties to local conditions during construction (Diefenderfer et al., 2006). Pavement temperature models may be coupled to additional models for temperature-dependent material properties and mechanical stress models (e.g. Bigl and Berg, 1996; Hermansson, 2001). To estimate the heat island effect of pavement surfaces, Asaeda and Ca (1993) developed detailed models for pavement and soil temperatures coupled with moisture transport. Previous studies of heat and moisture transport in soil have shown that transport of both liquid water and water vapor can be important processes in a soil heat budget (Sophocleous, 1979; de Vries, 1958).

In our study, a ground temperature model was developed to predict temperatures for vegetated and impervious surfaces with a spatial resolution on the order of 10 m and a temporal resolution on the order of 10 min. The emphasis on surface temperatures during rainfall events is different from other ground temperature model studies. The model formulation includes a description of all heat transfer pro-

cesses between the atmosphere and the ground surface, as well as the heat transfer between the ground surface and surface runoff. Surface temperatures during rainfall events and runoff temperature time series can be simulated. The model has been used successfully to simulate detailed surface temperature dynamics during individual rainfall events and continuous surface temperature time series over seven month periods for multiple years.

Temperature model for ground surfaces without vegetation cover

The basic ground surface temperature model is unsteady and one-dimensional, i.e. it considers only vertical heat fluxes and the vertical variation of temperature in the ground. The major components of the model are:

(1) Unsteady vertical heat conduction through a soil column with spatially varying thermal properties. Distinct surface layers such as asphalt, concrete, or gravel are assigned thermal properties (thermal conductivity, specific heat, density) separate from the underlying soil.
(2) A model for surface heat flux, based on surface properties (roughness, albedo, and emissivity) and weather conditions (e.g. solar irradiance, air temperature, wind speed, relative humidity or dewpoint temperature).

The model also includes a formulation for heat transfer between the ground surface and precipitation runoff during and after a rainfall event. As a result, the model can be used to simulate surface temperatures for a continuous sequence of dry and wet surface conditions/weather periods.

Unsteady vertical heat conduction in a soil column

Vertical soil temperature profiles are obtained in successive time steps of 1 h or less by solving the unsteady 1-D heat conduction equation using an implicit finite difference formulation. The model uses thin layers, e.g. 0.04 m, for pavements or the near-surface soil layers, and thicker layers, e.g. 1 m, towards the lower boundary of the soil column. As a result, good simulation results are possible with approximately 15 layers. The model does not presently include moisture-dependent thermal properties and advection of heat due to moisture movement.

The unsteady, 1-D heat conduction equation is

$$\frac{\partial T}{\partial t} = \frac{\partial}{\partial z}\left(D\frac{\partial T}{\partial z}\right) \tag{1}$$

where T is temperature, t is time, z is the depth coordinate, and D is the thermal diffusivity. Eq. (1) is discretized using a standard, implicit finite difference formulation (Patankar, 1980):

$$T_i^{j+1} = \left(\frac{D_{i-1,i}}{\delta z_{i-1}}T_{i-1}^j + \frac{D_{i,i+1}}{\delta z_i}T_{i+1}^j + \frac{\Delta z_i}{\Delta t}T_i^j\right)\left(\frac{\Delta z_i}{\Delta t} + \frac{D_{i-1,i}}{\delta z_{i-1}} + \frac{D_{i,i+1}}{\delta z_i}\right)^{-1} \tag{2}$$

where Δt is the time step, Δz is the layer thickness, and i and j are indices for depth and time dicretization, respectively, and δz is the node spacing. The thermal diffusivity, D, is assumed constant within each layer. The thermal diffusivity at the interface of two dissimilar materials, e.g. pavement and soil, is calculated using a harmonic mean (Patankar, 1980):

$$D_{i,i+1} = \frac{D_i D_{i+1}(\Delta z_i + \Delta z_{i+1})}{\Delta z_i D_{i+1} + \Delta z_i D_{i+1}}. \tag{3}$$

The boundary conditions for the soil temperature model include an adiabatic condition at the lower extreme of the soil column (nominally $z = 10$ m below the surface) and a surface heat flux boundary condition at zero depth, $z = 0$.

Heat flux across a ground surface

The net vertical heat transfer at the soil or pavement surface includes components due to long wave radiation, short wave (solar) radiation, evaporation, and convection. The surface heat transfer formulations used in this study are based on those given by Edinger et al. (1968, 1974) for lake and reservoir surfaces, but are applied to pavement and soil by adjusting parameters appropriately. Eqs. (4) through (11) give the formulations used to calculate the net surface heat flux, h_{net}.

The evaporative heat transfer formulation (Eq. (6)) uses the aerodynamic method to enable simulations at hourly time steps or less. For paved surfaces, the evaporative heat flux is calculated only when standing water is present. The evaporation and convection heat transfer components consider both forced convection, proportional to wind speed, and natural convection, related to the difference in temperature (density) of the air between the ground surface and the atmosphere. The wind velocity at 10 m height (u_{10}) is scaled by a sheltering coefficient (CS_h) to take into account the effect of trees, buildings, and topographical features on surface wind velocity (u_s). Incoming atmospheric long wave radiation (h_{lo}, Eq. (9)) is calculated based on air temperature (T_a) and cloud cover (CR).

$$h_{net} = h_{rad} - h_{evap} - h_{conv} - h_{ro} \tag{4}$$

$$h_{rad} = h_s + h_{li} - h_{lo} \tag{5}$$

$$h_{evap} = \rho_a L_v (C_{fc}u_s + C_{nc}\Delta\theta_v^{0.33})(q_{sat} - q_a) \tag{6}$$

$$h_{conv} = \rho_a c_p (C_{fc}u_s + C_{nc}\Delta\theta_v^{0.33})(T_s - T_a) \tag{7}$$

$$h_s = (1 - \alpha_s)R_s \tag{8}$$

$$h_{li} = \varepsilon\sigma(CR + 0.67 \cdot (1 - CR)e_a^{0.08})T_{ak}^4 \tag{9}$$

$$h_{lo} = \varepsilon\sigma T_{sk}^4 \tag{10}$$

$$U_s = CS_h u_{10} \tag{11}$$

where h_{net} is the total net surface heat transfer, h_{rad} is net radiation, h_s is the incoming short wave (solar) radiation, h_{evap} and h_{conv} are the evaporative and convective heat fluxes, respectively, ε and σ are the surface emissivity and the Stefan–Boltzmann constant, respectively, ρ_a is air density, c_p is the specific heat of water, L_v is the latent heat of vaporization, C_{fc} anf C_{nc} are coefficients for forced and natural convection, respectively, T_{ak} and T_{sk} are the absolute air and surface temperature (K), respectively, q_{sat} and q_a are the saturated and ambient specific humidity, respectively, $\Delta\theta_v$ is the difference in virtual temperature between the surface and atmosphere (Ryan et al., 1974), and α_s is the

surface albedo. Specific humidity, q, is related to vapor pressure, e, by: $q = 0.622\, e/(p - e)$, where p is atmospheric pressure. The outgoing long wave radiation (h_{lo}; Eq. (10)) is strongly dependent on surface temperature. A simple linearization (Eq. (12)) was used to maintain numerical stability at longer time steps:

$$h_{lo} = \varepsilon\sigma T_{sko}^4 + 4\varepsilon\sigma T_{sko}^3 (T_{sk} - T_{sko}) \tag{12}$$

where T_{sk} and T_{sko} are the value of the surface temperature (K) for the current and previous time steps. The convective and evaporative heat flux components are linearized in a similar manner.

Heat flux across a wet ground surface

Surface heat flux due to precipitation and a water surface layer (with or without runoff) is estimated based on the difference between the current surface temperature and the precipitation temperature. This heat flux component gives the thermal coupling between the surface runoff and the ground surface. It is assumed that (1) the precipitation temperature is the dew point temperature, and (2) the runoff water and the ground surface equilibrate to the same temperature over the time step (Δt), i.e. the water layer is vertically well mixed. To achieve this equilibrium, a conductive heat flux h_{ro} can be calculated which draws heat out of a thin layer of pavement at the surface with thickness δ. The thickness δ is estimated from the thermal properties of the pavement and the time step, based on analytic solutions for heat conduction into an infinite slab subject to a change in surface temperature (Eckert and Drake, 1972):

$$\delta = \sqrt{12 \cdot D \cdot \Delta t}, \tag{13}$$

Eq. (13) is derived for a uniform initial temperature distribution. Since the heat conduction equation is linear for constant material properties, it is assumed that the solution may also be used to consider an incremental change in an arbitrary temperature profile, as in Fig. 1. For a time step of 15 min and a thermal diffusivity of 4×10^{-6} m^2/s, the layer thickness δ = 0.2 m. An equation for the heat balance for the water layer and the pavement may then be written as:

$$h_{ro} = i(\rho c_p)_w (T_s - T_{dp}) = -\frac{\delta}{2\Delta t}(\rho c_p)_p (T_s - T_{so}) \ \text{(W/m}^2\text{)} \tag{14}$$

where T_s and T_{so} are the current and previous surface temperature, respectively, i is the precipitation rate, and $(\rho c_p)_p$ and $(\rho c_p)_w$ are (density specific heat) for the pavement and water, respectively. The factor (δ/2) takes into account that the temperature change in the pavement decreases with depth, whereas the temperature change in the water layer is assumed to be uniform across its thickness. If the dew point temperature, the initial surface temperature, and the precipitation rate, i, are known, Eq. (14) can be rearranged to solve for h_{ro} in terms of known quantities:

$$h_{ro} = i(\rho c_p)_w (T_{so} - T_{dp}) \left(\frac{\beta}{1+\beta}\right); \quad \beta = \frac{\delta(\rho c_p)_{pave}}{2P(\rho c_p)_{water}}. \tag{15}$$

The heat flux from the soil across the ground surface (z = 0) to the water layer (runoff) may be estimated using Eq. (15) for each time step based on the precipitation depth. This heat flux is added algebraically to the atmospheric heat flux components. The resulting ground surface temperature also represents the water layer or runoff temperature. If a water layer depth is known from the previous time step, the thermal mass associated with it can be added to the thermal mass of the top layer of the ground in the heat conduction model. This residual water layer is not included in Eq. (15), since it has already been heated to the surface temperature.

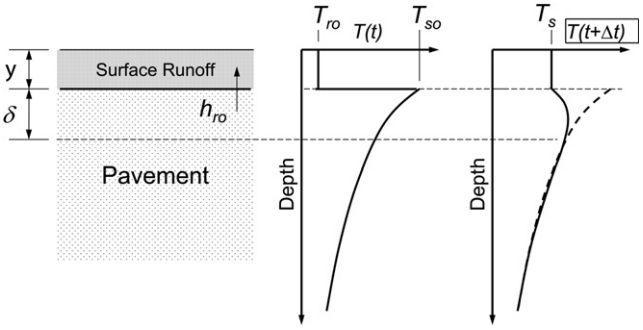

Figure 1 Schematic of the formulation for heat transfer between surface runoff and the underlying pavement. Example temperature profiles show the temperatures in the pavement prior to a rainfall event ($T(t)$) and after a rainfall event ($T(t + \Delta t)$, where the initial surface temperature (T_{so}) has equilibrated with the initial runoff temperature (T_{ro}) to yield the new surface and runoff temperature (T_s).

A lateral variation in runoff depth leads to a small lateral temperature gradient, which is not addressed in the present model. However, a typical runoff depth of a few mm represents an insignificant thermal mass compared to the thermal mass of soil or pavement with thickness δ.

Soil moisture model

For application to pervious land surfaces, the soil temperature model includes a component for soil moisture. Soil moisture is modeled over depth using the same discrete layers as the thermal model. The transport of moisture between layers is modeled as a wetting front with a discretized version of Darcy's law:

$$\frac{\Delta D_i}{\Delta t} = \bar{K}\left(1 + \frac{\Phi_{i+1} - \Phi_i}{\delta z_i}\right) \tag{16}$$

where $\Delta D/\Delta t$ is the Darcy velocity of the water moving between layers i and i + 1 in the time step Δt, $\bar{K}$ is the average hydraulic conductivity, Φ is potential (head), and δz_i is the distance between the center of layers i and i + 1. The average hydraulic conductivity and potential in each layer is estimated from the soil water content θ from the previous time step:

$$K_i = K_s \left(\frac{\theta_i}{\theta_s}\right)^{2b+3} \tag{17}$$

$$\Phi_i = \Phi_b \left(\frac{\theta_i - \theta_{wp}}{\theta_s - \theta_{wp}}\right)^{-b} \tag{18}$$

where K_s is the saturated hydraulic conductivity, θ_i is the soil moisture in the previous time step, θ_s is the saturated soil water content, Φ_b is the bubbling pressure head, θ_{wp} is the

wilting point soil moisture, and b is a soil specific constant. For pervious surfaces, the evaporative heat flux (Eq. (6)) is adjusted based on the soil moisture content at the surface:

$$h_{evap} = \rho_a L_v \theta' (C_{fc} u_s + C_{nc} \Delta \theta_v^{0.33})(q_{sat} - q_a) \quad (19)$$

where $\theta' = (\theta - \theta_{fc})/(\theta_s - \theta_{fc})$, θ is the soil moisture content, θ_{fc} is the field capacity, and θ_s is the saturated soil water content. The infiltration rate, f, is calculated using the Green–Ampt formulation:

$$f = K\left(\frac{\Phi_b(\theta_s - \theta) + F}{F}\right) \quad (20)$$

where F is the cumulative infiltration depth for the rainfall event, i.e. $F = \Sigma(f \cdot \Delta t)$. The solution to Eq. (20) is obtained using a linearized solution form given by Li et al. (1976). Infiltration is calculated based on the precipitation, i.e. the precipitation depth is the maximum possible infiltration. If precipitation exceeds infiltration, the remaining water is assumed to be removed from the system by runoff at the end of each time step. This simple approach was found to be sufficient for the purposes of simulating surface temperature, but it would not accurately simulate infiltration for areas of land with runoff time constants much greater than the analysis time step (15 min).

Simulated temperatures of paved surfaces

The bare surface temperature model was calibrated and verified using recorded weather data as model input, and measured pavement temperature data for concrete and asphalt test sections from the MnROAD facility near Albertville, MN. Eight years (1998–2005) of 15 min climate data were available, six years of asphalt temperature data and one year of concrete temperature data (2004). The precipitation received on the pavement is assumed to completely run off in each time step, so that no standing water is carried over to the next time step, and infiltration is assumed to be zero. The simulations were run for the time period April 1st–September 30th of each year using either a 15 min or 60 min time step and a total soil depth of 10 m.

Calibrated parameter values

The parameter values in Table 1 were obtained by minimizing the root–mean–square error (RMSE) of the simulated and measured pavement temperature values for the upper-most thermistor node (2.5 cm below the surface).

Parameter sensitivity analysis

The sensitivity of the simulated surface temperatures to several key input parameters is given in Table 2. The emissivity of the pavement had the most influence on pavement surface temperature. An increase in emissivity caused a proportionate and rather uniform decrease in surface temperature, i.e. both the daytime and nighttime temperatures decreased. The simulated pavement surface temperatures were relatively insensitive to the sub-soil parameters.

Comparison of simulated and measured pavement temperatures

Simulated and measured asphalt and concrete surface temperatures agreed closely for all snow-free months using either 15 min or 60 min time steps. Table 3 summarizes

Table 1 Calibrated parameter values for asphalt, concrete and bare soil

Parameter	Description	Asphalt	Concrete	Bare soil
α	Solar albedo	0.12	0.20	0.15
C_{fc}	Surface heat/moisture transfer coefficient for forced convection	0.0015	0.0015	0.003
C_{nc}	Coefficient for natural convection	0.0015	0.0015	0.0015
CS_h	Wind sheltering coefficient	1.0	1.0	1.0
ε	Pavement emissivity	0.94	0.94	0.95
ρC_p (J/m^3/°C)	Density specific heat pavement	2.0e06	2.0e06	2.4e06
D_{pav} (m^2/s)	Pavement thermal diffusivity	4.0e−07	7.0e−07	N/A
D_{soil} (m^2/s)	Soil thermal diffusivity	6.0e−07	6.0e−07	6.0e−07

Table 2 Sensitivity of simulated daily surface temperature parameters to model input parameters for the asphalt test section

	Average (°C)	Maximum (°C)	Minimum (°C)	Amplitude (°C)
ε	−0.497	−0.422	−0.437	0.015
CS_h	−0.266	−0.516	−0.032	−0.484
C_{nc}	−0.240	−0.398	−0.113	−0.285
C_{fc}	−0.234	−0.405	−0.079	−0.326
α	−0.104	−0.166	−0.034	−0.132
D_{pav}	−0.010	−0.060	0.087	−0.146
$(\rho C_p)_{pav}$	0.010	−0.438	0.466	−0.904
D_{soil}	0.009	−0.060	0.068	−0.128

Each value in the table is the change in surface temperature, °C, for a 10% increase in the input parameter listed in the first column.

Table 3 Summary of temperature simulation accuracy for different land uses, where r^2 and the overall RMSE gives the simulation error for the entire 1 h simulated time series

Land use	Year	r^2	RMSE overall (°C)	RMSE daily maximum (°C)	RMSE daily minimum (°C)
Asphalt	2000	0.982	1.60	1.85	1.31
Asphalt	2001	0.981	1.58	2.52	1.43
Asphalt	2002	0.970	1.85	2.28	1.57
Asphalt	2003	0.980	1.44	2.13	1.51
Asphalt	2004	0.981	1.38	2.07	1.32
Asphalt	2005	0.962	1.73	1.90	1.27
Bare soil	2004	0.951	1.95	2.74	1.19
Concrete	2004	0.981	1.74	1.52	1.76
Corn	1999	0.967	1.28	1.88	0.95
Forest	2004	0.944	0.76	1.02	1.09
Tall grass	2005	0.978	0.97	1.01	0.86
Lawn	2004	0.925	1.72	1.65	1.68
Soybeans	2000	0.971	1.00	1.39	0.83

Table 4 Simulation error (RMSE, °C) of 1 h surface temperature, by month, for different land uses

Land use	Year	April	May	June	July	August	September
Asphalt	2004	1.36	1.42	1.52	1.58	1.50	1.74
Bare soil	2004	1.66	1.54	1.85	2.08	2.23	2.24
Concrete	2004	1.25	1.93	1.24	1.23	2.29	2.11
Corn	1999	1.53	1.4	1.06	0.94	1.27	1.42
Forest	2004	0.71	0.79	0.53	0.95	0.79	0.68
Lawn	2004	1.69	1.54	1.81	1.9	1.35	1.97
Soybeans	2000	1.32	1.15	0.75	1.08	0.87	0.67
Tall grass	2005	1.48	0.88	1.03	0.93	0.90	

the accuracy of the 60 min temperature simulations (r^2, RMSE) for the entire simulation period, while Table 4 gives the variation of RMSE (root—mean—square error) by month. The model was calibrated with 2004 data, but worked almost as well for the other five years. Fig. 2 gives time series of simulated and measured surface temperatures for asphalt surfaces in June/July of 2004. Fig. 3 is a plot of simulated versus measured asphalt surface temperatures for (1) both wet and dry weather conditions and (2) wet weather only. The values plotted are 1 h averaged values of the raw 15 min simulated and observed data. In both cases, the slope of the relationship in Fig. 3 is close to 1:1 and the intercept is near zero (less than 1 °C on each axis). For 2004, the RMSE for wet weather was 1.1 °C, compared to 1.4 °C for all weather.

Surface heat flux during rainfall events

Surface temperatures and surface heat flux components during wet weather are of particular interest for paved surfaces, because the surface heat flux raises or lowers the runoff temperature. Fig. 4 gives time series of the simulated heat flux components during an observed 3.8 cm rainfall event on June 20, 2005. The observed air temperature, dew point temperature, and precipitation were taken from the MNROAD weather station in Albertville, MN. Prior to the rainfall event, four heat flux components are significant: incoming long wave radiation, outgoing longwave (back radiation), solar, and convection. During the rainfall event, both evaporation and the runoff conduction become significant, while convection and solar radiation become less significant. For all rainfall events in the 2005 climate series, the average net surface heat transfer rate was −186 W/m^2, the (−) sign indicating a surface cooling. Of this net heat flux, convective heat flux contributed 17%, evaporative heat flux 31%, conduction to the runoff 43%, and net radiation 9%, with all components tending to cool the pavement surface.

Simulated temperatures of bare soil surfaces

Compared to a pavement, a bare soil is more complex to model, because it is porous, permeable, and contains water. Evaporation contributes to the surface heat flux during both wet and dry weather. The bare soil temperature model was validated with observed soil temperature data from the University of Minnesota St. Paul campus, where a bare soil plot is maintained. There is a slight uncertainty in the depth of observed temperature sensors near the surface because erosion and deposition can change the sensor depths over time.

Calibrated parameter values

Bare soil temperature was simulated for the period April 1 to September 30, 2004, using 1 h climate data from the University of Minnesota St. Paul campus. Calibrated parameter values that gave the best fit of simulated to measured bare

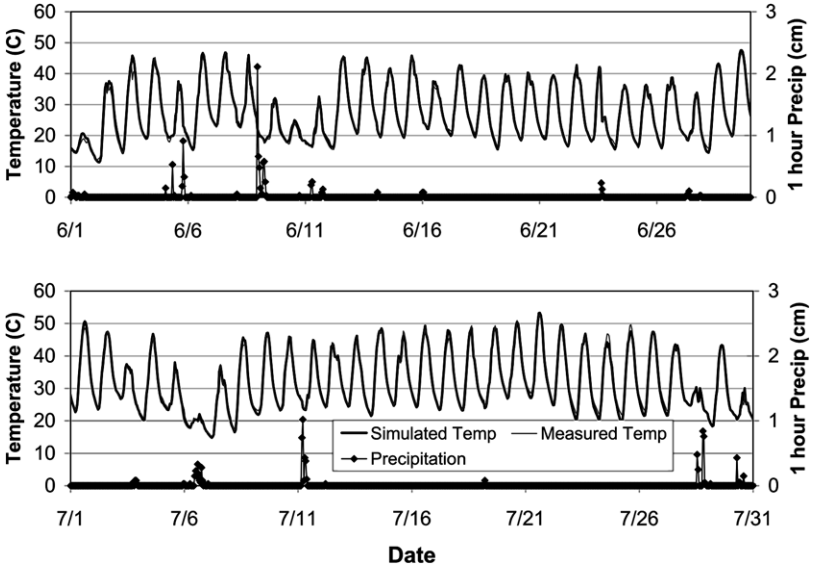

Figure 2 Simulated and measured pavement temperature (2.5 cm depth) and measured precipitation for June and July, 2004, MNROAD test sections 33 (asphalt), for 15 min time step plotted as 1 h averages.

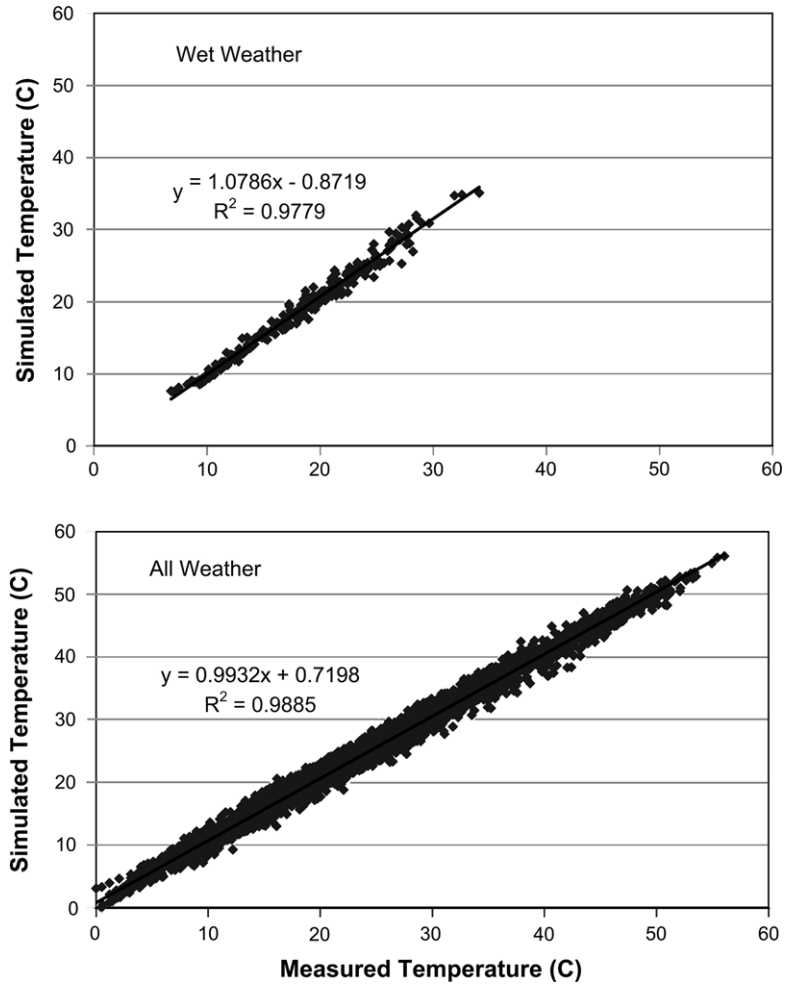

Figure 3 Simulated versus measured hourly pavement temperatures (2.5 cm depth) for April—September, 2004, MNROAD test section 33 (asphalt). The lower panel contains all data points for the period (n = 16,780), while the upper panel displays data points for wet weather only (n = 579).

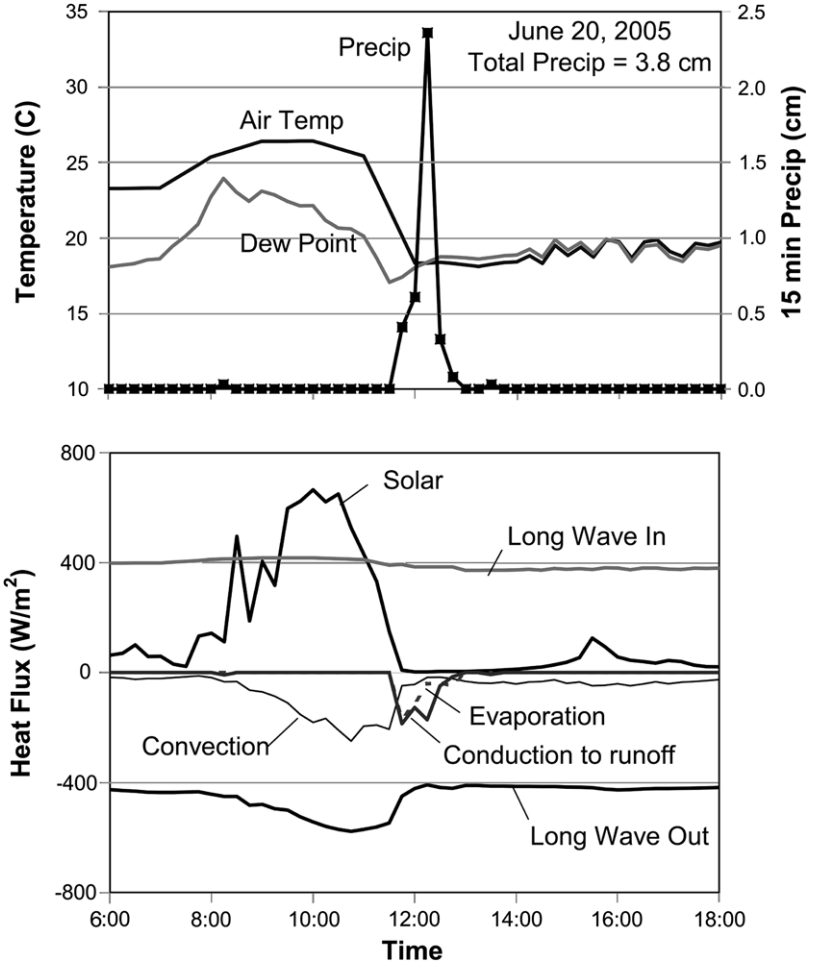

Figure 4 Time series of simulated heat flux components for an asphalt surface during an observed rainfall event on June 20, 2005. Additional associated climate data are given in the upper panel.

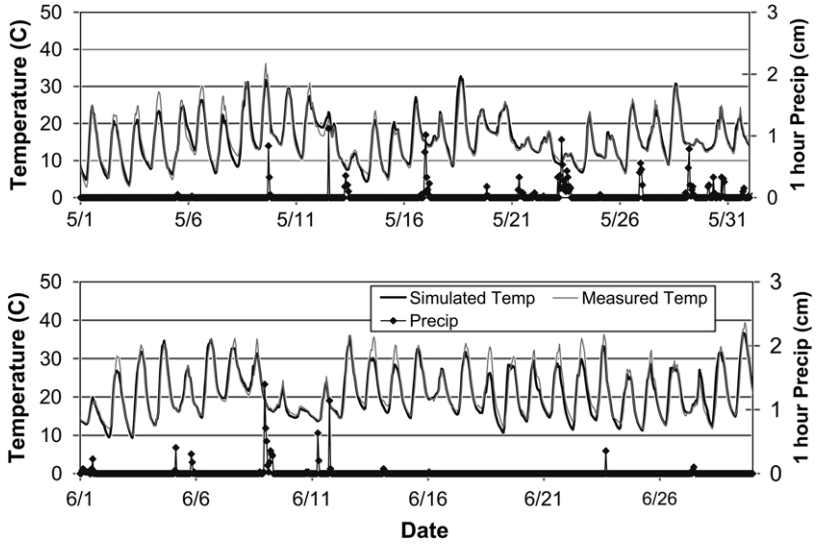

Figure 5 Simulated and measured bare soil temperature (1 cm depth) and measured precipitation for May—August, 2004, St. Paul campus bare soil plot, 1 h time step.

soil surface temperature are given in Table 1. The calibration was made with weather data from the summer of 2004. Calibrated parameter values for bare soil surfaces are similar to those for pavements, except the forced con-

vection coefficient (C_{fc}) is double for bare soil due to higher roughness.

Comparison of simulated and measured bare soil surface temperatures

The overall RMSE values are higher for the bare soil (1.9 °C) compared to the 2004 pavement simulations (1.4 °C). Table 4 summarizes the errors for the bare soil surface temperature simulation by month. The RMSE generally increases slightly over the season, from 1.6 to 2.2 °C. Examination of the simulated and measured temperature time series (Fig. 5) shows that the simulated surface temperature both over-predicts and under-predicts peak daily temperature during different periods of the season — this behavior may be due to errors in the simulated soil moisture. Although the soil moisture model appears to give reasonable results (Fig. 6), no field data are available to calibrate the model for the St. Paul plot.

Temperature model for ground surfaces with a plant cover

The introduction of a plant canopy has several major effects on the surface heat transfer and temperature of the underlying soil:

(1) The amount of short wave radiation reaching the soil/water surface is reduced by shading.
(2) The plant canopy absorbs long wave radiation from the sky and re-radiates to the underlying soil/water surface.
(3) Convective and evaporative heat fluxes at the ground surface are reduced by wind sheltering. Evaporation from the soil/water surface is largely replaced by plant transpiration, which is not directly associated with a heat flux component at the soil surface.

To adequately model the effect of a plant canopy on the net long wave radiation reaching the soil/water surface, it is necessary to write an additional and separate heat budget equation for the plant canopy and to solve the equation for a canopy temperature.

Formulation of plant canopy model

Modeling the heat and mass transfer properties of plant canopies is a topic of ongoing studies, mainly for application to crop growth research and climate modeling. The plant canopy model used in this study is based on the work of Deardorff (1978) and Best (1998). Deardorff (1978) published a relatively complex model for soil temperature beneath a plant canopy. The model includes a separate heat balance equation for the plant canopy, a canopy temperature, and a distinct air temperature and humidity within the canopy. The canopy model used in this study is similar to the model used by Best (1998), a simplified version of the Deardorff model. The convective and evaporative heat flux components between the ground and the canopy are assumed to be negligible, eliminating the need to calculate a separate air temperature and humidity within the plant canopy.

The heat flux components considered in the plant canopy model are illustrated in Fig. 7, and the corresponding heat balance equation for the canopy is given by Eq. (21). It is assumed that the canopy has negligible heat capacity, so that heat flux components exactly balance each other during each time step. Expressions for the heat flux components are given in Eqs. (22)—(25). The net atmospheric radiation, $h_{rad,a}$, includes incoming long wave radiation, h_{li}, previously given by Eq. (9). Note that all heat flux components are scaled by the vegetation density, v, which varies from 0 to 1, where $v = 1$ corresponds to a leaf area index of approximately 7 (Deardorff, 1978):

$$h_{rad,a} - h_{rad,g} - h_{evap,f} - h_{conv,f} = 0 \quad (21)$$

$$h_{rad,a} = (1 - \alpha_f) v R_s + v h_{li} - v \varepsilon_f \sigma T_{fk}^4 \quad (22)$$

$$h_{rad,g} = v \varepsilon_f \sigma T_{fk}^4 - v \varepsilon_g \sigma T_{sk}^4 \quad (23)$$

$$h_{evap,f} = \rho_a L_v v (q_{sat}(T_f) - q_a)/(r_a + r_s) \quad (24)$$

$$h_{conv,f} = \rho_a c_p v (T_f - T_a)/r_a \quad (25)$$

where $h_{rad,g}$, is the net radiative flux between the canopy and the ground, $h_{evap,f}$ and $h_{conv,f}$ are the canopy evaporative and convective heat fluxes, α_f is canopy albedo, ε_f and ε_g are the canopy and ground emissivity, T_f and T_{fk} are the canopy temperature in (°C) and (K), q_a and q_{sat} are the ambient and saturated specific humidity. The aerodynamic (r_a) and stomata (r_s) resistance coefficients are calculated using expressions similar to those of Deardorff (1978):

$$r_a = 1/(c_f u_s) \quad (26)$$

$$c_f = 0.01(1 + 0.3/u_s) \quad (27)$$

$$r_s = 200(R_{s,max}/(R_s + 0.03 R_{s,max}) + (\theta_{wp}/\theta)^2) \quad (28)$$

where c_f is a transfer coefficient and $R_{s,max}$ is the maximum solar radiation.

The formulation for the ground surface heat flux is similar to those used for bare soil and pavements, except that the heat flux components are reduced as the canopy density is increased. The constant C_e establishes the level of soil evaporation for fully dense canopies, e.g. setting $C_e < 1$ gives non-zero soil evaporation for the full canopy case. The heat balance for the ground surface is given by Eq. (29), and the heat flux components are specified by Eqs. (30)—(32):

$$h_{net,g} = h_{rad,net,g} - h_{evap,g} - h_{conv,g} - h_{ro} \quad (29)$$

$$h_{rad,net,g} = (1 - \alpha_g)(1 - v) R_s + (1 - v) h_{li} + v \varepsilon_f \sigma T_{fk}^4 - \varepsilon_g \sigma T_{sk}^4 \quad (30)$$

$$h_{conv,g} = \rho_a c_p (1 - C_e v)(C_{fc} u_s + C_{nc} \Delta \theta_v^{0.33})(T_s - T_a) \quad (31)$$

$$h_{evap,g} = \rho_a L_v \theta' (1 - C_e v)(C_{fc} u_s + C_{nc} \Delta \theta_v^{0.33})(q_{sat}(T_s) - q_a) \quad (32)$$

where $h_{rad,net,g}$, $h_{conv,g}$ and $h_{evap,g}$ are the net radiative, convective, and evaporative heat flux at the ground surface, respectively, and α_g is ground albedo. To calculate the surface heat flux for each time step, Eqs. (21)—(28) are used to find a canopy temperature, based on values of air temperature, solar radiation, dew point, and wind speed. Since Eq. (23) is non-linear in canopy temperature (T_f), it is solved using Newton's method. The calculated canopy temperature is then used to calculate the ground surface heat flux and its components using Eqs. (29)—(32). The soil evaporation and canopy evaporation are used to update the soil

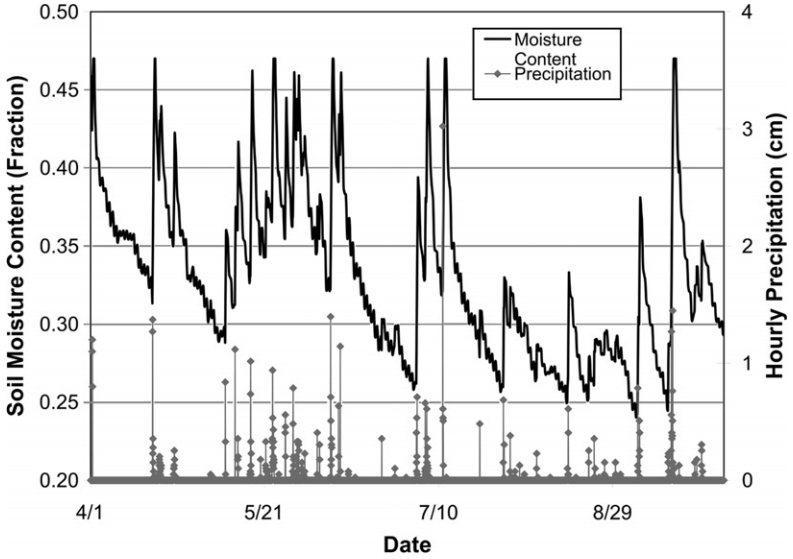

Figure 6 Simulated soil moisture content in surface layer and precipitation versus time for bare soil plot at St. Paul campus, April—September, 2004.

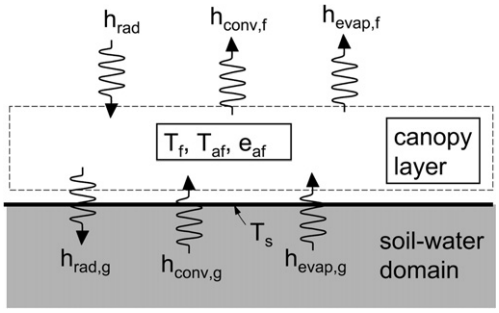

Figure 7 Major heat flux components for the plant canopy model.

moisture content. Canopy interception is not included in the water budget analysis.

Calibration and validation of the model for vegetated ground surfaces

The plant canopy model described in 'Formulation of plant canopy model' section was inserted in the basic soil temperature model and calibrated for five different vegetation types: mowed grass, grass rangeland, corn, soybeans, and forest, using the data sources listed in Table 5. The goal was to achieve good simulations of soil temperature while minimally changing the model parameters between the different sites. For all five sites, it was possible to simulate the different vegetation types by changing only the canopy density parameter, ν, the soil heat capacity, ρC_p, and the canopy albedo, α_f.

Table 6 gives the values of the nominal (precalibration) parameter set. These values were chosen from published values and then adjusted to give good overall results for all sites. Table 7 summarizes the simulation accuracy of near-surface soil temperature for the five sites. RMSE (root—mean—square error) values are given for simulations with the nominal (uncalibrated) parameter set (Table 6), i.e. no parameter adjustment for each site and simulations with calibrated parameters for each site (Table 7).

Soil temperature sensitivity to canopy model parameters

The sensitivity of the simulated soil surface temperatures to several key input parameters in the canopy model is given in Table 8. Overall, the emissivity of the foliage and soil had the most influence on surface temperature, with roughly equal and opposite effects, followed by the vegetation density (ν) and the soil evaporation/convection scaling parameter (C_e). An increase in foliage emissivity or a decrease in soil emissivity caused an increase in both day and night soil surface temperatures, with relatively little effect on the diurnal amplitude. The soil surface temperature was relatively insensitive to the foliage albedo and the soil thermal and hydraulic parameters. Introducing a small amount of soil evaporation and convection, i.e. decreasing C_e from 1.0 to 0.9, caused a measurable decrease in soil temperature (0.5 °C).

Simulated soil surface temperatures below different types of plant covers

The soil temperature model was tested using measured soil temperatures beneath different plant covers. In all cases, observed soil temperatures were point measurements using discrete temperature probes. It was assumed, therefore, that these point measurements were in locations representative of the typical cover.

Lawns and tall grass prairie

Soil temperature data from a grass plot at the University of Minnesota St. Paul campus and from an Ameriflux site at Batavia, Illinois were used to test the soil/vegetation temperature model. The grass plot in St. Paul is representative

Table 5 Summary of data sites and sources used for validating the canopy model

Location	Vegetation type	Year	Source
Bondville, IL	Corn	1999	[a]
	Soybeans	2000	
Batavia, IL	Tall grass prairie	2005	
Mount Mansfield, VT	Forest	2004	[b]
St. Paul, MN	Mowed Grass	2004	[c]

[a] Ameriflux network (http://public.ornl.gov/ameriflux/).
[b] Natural resources conservation service soil and climate analysis network (http://www.wcc.nrcs.usda.gov/scan).
[c] University of Minnesota, Department of Soil, Water and Climate.

Table 6 Nominal uncalibrated parameter values used for all simulations, except where noted in Table 7 and in the text

Parameter	Value	Parameter	Value
C_e	1	α_f	0.20
C_{Hf}	0.02 m	ε_g	0.94
C_{fc}	0.0015 m	ε_f	0.95
C_{nc}	0.0015 m	$(\rho C_p)_{soil}$	2.5e06 J/m^3/°C
D_{soil}	4.0e−07 m^2/s	v	1
α_s	0.12		

Table 7 Summary of RMSE values from simulations with uncalibrated and calibrated parameter values

Location	Plant type	RMSE (°C) uncalibrated	RMSE (°C) calibrated	Calibration parameter (value)
Batavia, IL	Tall grass prairie	1.7	1.0	v (0.95) α_f (0.25) $(\rho C_p)_{soil}$ (2.2e06 J/m^3/°C)
Bondville, IL	Corn	3.5	1.3	*v (0.6–0.95)* $(\rho C_p)_{soil}$ (2.0e06 J/m^3/°C)
Bondville, IL	Soybeans	2.5	1.0	*v (0.4–1.0)* $(\rho C_p)_{soil}$ (2.0e06 J/m^3/°C)
Mount Mansfield, VT	Forest	0.9	0.8	*v (0.6–1.0)*
St. Paul, MN	Mowed grass	1.7	1.7	None

The calibrated parameters and their (values) are given for each site in the last column. The values are fixed or seasonally varied for each site.

Table 8 Sensitivity of simulated daily surface temperatures to model input parameter values for the St. Paul grass plot

	Average (°C)	Maximum (°C)	Minimum (°C)	Amplitude (°C)
ε_f	6.07	6.22	5.91	0.32
ε_g	−5.69	−5.77	−5.58	−0.19
v	−1.07	−2.43	0.00	−2.43
C_e	0.52	0.45	0.62	−0.17
D_{soil}	−0.11	−0.25	0.03	−0.28
α_f	−0.05	−0.06	−0.03	−0.03
$(\rho C_p)_{soil}$	−0.04	−0.10	0.02	−0.12
C_{Hf}	−0.04	−0.08	0.00	−0.08
K_s	0.00	0.00	0.01	0.00

Each value in the table is the change in surface temperature (°C) for a 10% increase in the input parameter listed in the first column. If the nominal parameter value is the maximum value, e.g. $v = 1$, the value was decreased by 10% and the resulting response multiplied by −1. K_s is the saturated hydraulic conductivity of the soil.

of a mowed lawn, while the grass plot at Batavia is representative of tall grass prairie. For both grass plots, the best agreement of simulated and measured soil temperatures was obtained using a full canopy (v = 0.95—1.0) and no soil evaporation/convection (C_e = 1). For the St. Paul grass plot, good agreement between measured and simulated soil temperatures was obtained (Table 3) when the soil parameters were the same as used for the bare soil plot, and foliage parameters were within the expected range, i.e. ε_f = 0.95, α = 0.20, C_{Hf} = 0.02. The calibrated values of the soil and foliage parameters used for the tall grass plot in Batavia are given in Table 7. Using the St. Paul vegetation and soil parameters produced reasonable simulation results for the Batavia tall grass plot, but minor adjustments to the canopy density, canopy albedo, and soil heat capacity improved the overall simulation RMSE from 1.7 °C to 1.0 °C. Tables 3 and 4 give overall and monthly RMSE values for both grass plots. For the short grass, there is little systematic seasonal variation in RMSE, while the tall grass shows better RMSE later in the season. Overall a better fit between simulations and measurements is achieved for the tall grass.

Time series plots of measured and recorded soil surface temperatures for June 2004 in Fig. 8 show slightly higher soil surface temperatures and diurnal amplitudes in the tall grass site, which is about 250 km south of the short grass site.

Row crops

To evaluate the vegetation/soil temperature models ability to simulate agricultural land use, the model was applied to an Ameriflux data set for Bondville, IL, just west of Urbana/Champaign. The crop on the instrumented test plot is rotated each year between corn and soybeans. Data are available from 1996 to present, including climate data and soil temperatures. Data from 1999 (corn) and 2000 (soybeans) were selected for model evaluation, based on the completeness of the data files for these years.

Application of the vegetation/soil temperature model with the nominal parameter set (Table 6) lead to an over-prediction of maximum surface temperatures in April and May, and relatively high RMSE values (Table 7). Better simulation accuracy was achieved by introducing a seasonally varying canopy density, with slightly different characteristics for the corn and soybean crops (Fig. 9). In addition, reducing the scaling constant C_e to 0.5, i.e., setting evaporation and convection to 50% of the bare soil value, further increased the simulation accuracy. This suggests that a field that has been plowed and planted with a row crop may have significant evaporation from the soil, even with a relatively dense plant canopy.

With these changes in parameter values, good agreement of measured and simulated surface temperatures was achieved for the entire period (Table 3 and 4). Examples of simulated and measured soil temperature time series for the corn crop are compared in Fig. 10 for June and July, 1999.

Table 3 and 4 summarize the overall error coefficients. The RMSE is quite low, 1.3 °C for corn and 1.0 °C for soybeans. Maximum soil surface temperatures for the corn crop approach 40 °C early in the growing season. This is higher than for the grass plot, and is attributed to the reduced canopy coverage in the early part of the year (Fig. 9); more solar heat flux reaches the soil surface. By comparison, the soybean canopy developed more rapidly in the growing season and produced maximum soil temperatures of about 30 °C, close to those measured at the St. Paul grass plot.

Forests

The vegetation/soil temperature model was applied to forested ground cover using data from a SCAN site at Mount Mansfield, VT with forest cover. The nominal parameter values given in Table 6 were used, except for vegetation density (Fig. 9), which was made seasonally varying to represent an under story plus the seasonal development of a deciduous tree canopy. The simulated soil temperatures at 5 cm depth agreed with observed values to an overall RMSE of 0.76 °C (Table 3 and 4 and Fig. 11). Simulated surface tem-

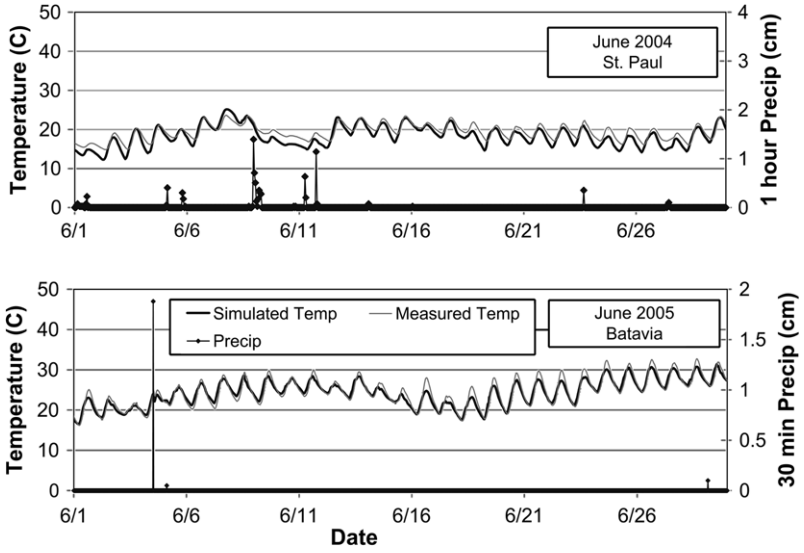

Figure 8 Time series of simulated and measured near-surface soil temperatures and measured precipitation for grass plots at St. Paul (upper panel) and at Batavia, IL (lower panel).

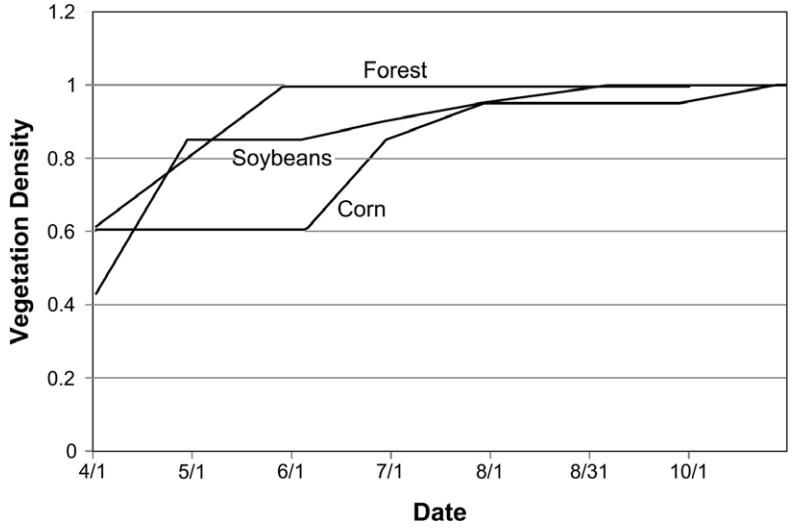

Figure 9 Calibrated seasonal variation of canopy density (ν) for corn, soybeans, and forest.

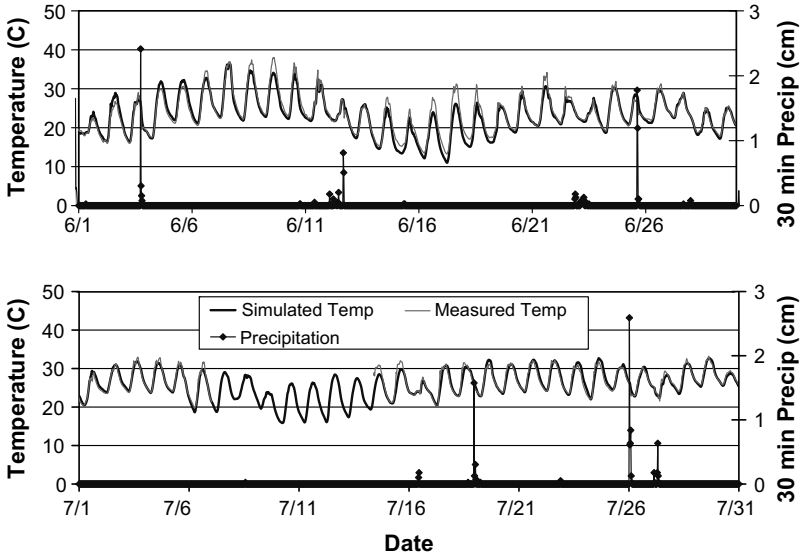

Figure 10 Simulated versus measured soil temperature (1 cm depth) and measured precipitation, June—July 1999, at the Bondville, IL, site with corn crop, 30 min time step.

peratures did not exceed 20 °C for the period of simulation (April—October 2004), which may be attributed to the vegetation canopy and the relatively low air temperatures for the higher altitude site (680 m or 2200 ft).

Comparison of ground temperatures for different surface covers

Ground surface temperatures have been simulated for a variety of surface covers, including pavements, bare soil, short and tall grass, trees and agricultural crops. However, the simulations were run for different locations and different years as imposed by the availability of measured soil temperature and climate data. To clarify the variation in surface temperatures for the different land uses, the calibrated coefficients for each land use were used to simulate surface temperatures using the same climate data set from Albertville, MN and the same soil coefficients. Simulations were performed for seven land uses, for six years of 15 min climate data, from April 1 through October 31 in each year (1998—2000, 2003—2005).

The results are given as the seasonal variation of weekly averaged soil surface temperatures (Fig. 12) and in a summary table by month (Table 9). The values in each sub-section of Table 9 are sorted by the seasonal average temperature for each land use. July gives the highest average temperature for all land uses. For averaging all weather conditions (wet and dry), asphalt and concrete clearly give the highest average temperature in each month. Asphalt gives the highest average daily maximum and average daily amplitude. Short and long grass, corn, soybeans and forest

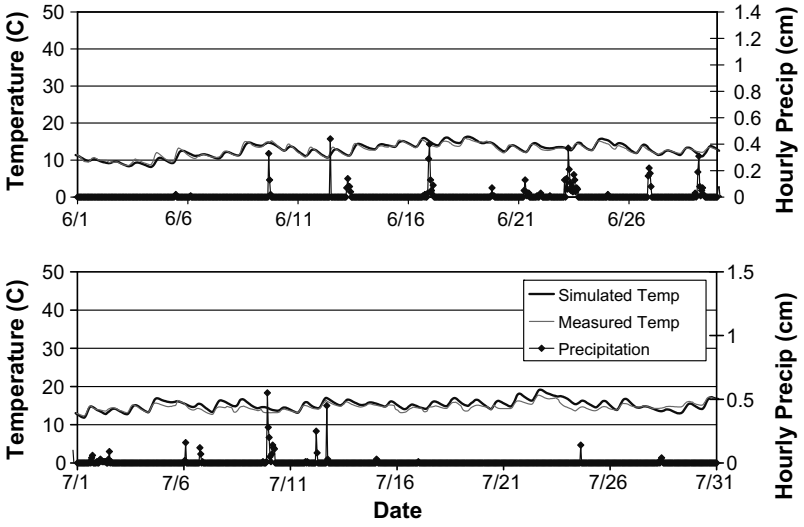

Figure 11 Simulated versus measured soil temperature (5 cm depth) and measured precipitation, July 2004, at the Mount Mansfield, VT forest plot.

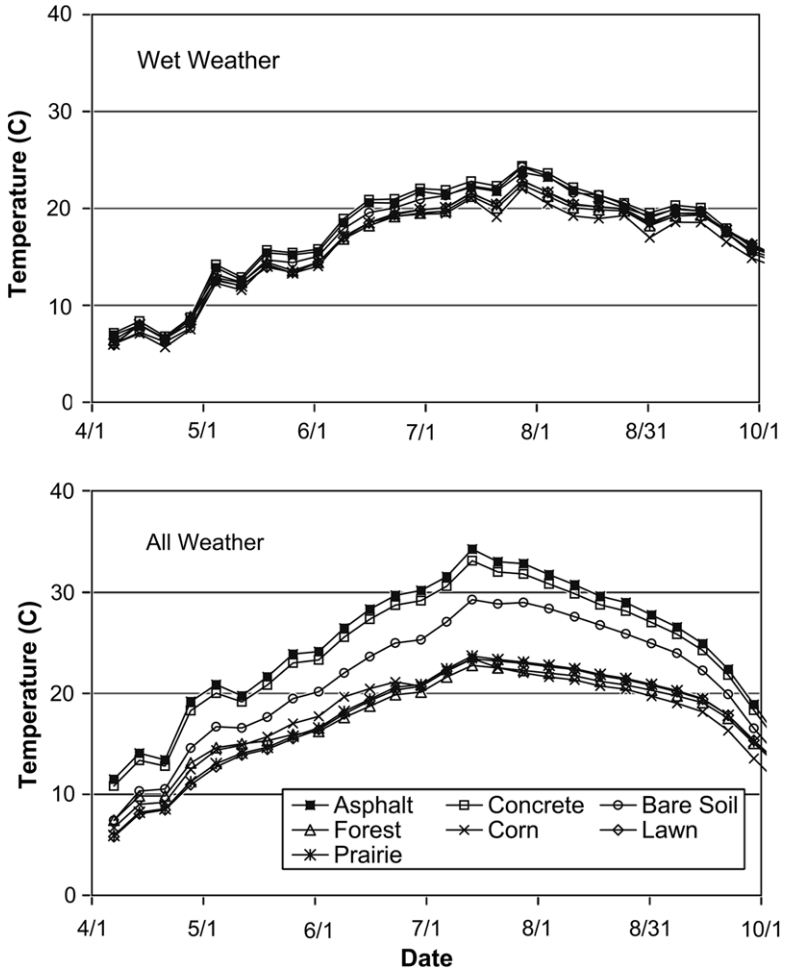

Figure 12 Simulated average weekly surface temperatures for seven land uses using 6 years of 15 min climate data from the MnROAD site in Albertville, MN as model input. The lower panel gives results for both dry and wet weather, while the upper panel gives results for wet weather only.

Table 9 Simulated monthly average surface temperature, average daily maximum and average daily minimum for seven ground covers using 6 years of 15 min climate data from Albertville, MN

	April	May	June	July	August	September	October	All
Average monthly surface temperature (°C)								
Asphalt	14.7	22.1	28.1	32.9	29.7	23.4	13.7	23.5
Concrete	14.0	21.3	27.1	31.9	28.8	22.8	13.2	22.7
Bare soil	10.9	18.1	23.5	28.6	26.6	20.9	12.1	20.1
Tall Grass	8.6	14.9	19.4	23.1	21.9	18.3	11.7	16.8
Forest	10.2	15.5	18.7	22.3	21.2	18.0	11.7	16.8
Lawn	8.5	14.6	19.2	22.9	21.8	18.3	11.8	16.7
Corn	9.5	16.0	20.1	22.5	20.7	16.9	10.1	16.6
Average monthly surface temperature, wet weather (°C)								
Concrete	7.6	14.4	20.0	22.9	21.4	18.7	12.9	16.8
Asphalt	7.3	14.2	19.6	22.3	21.0	18.4	12.8	16.5
Bare soil	6.7	13.6	19.0	22.4	21.1	18.3	12.4	16.2
Lawn	7.1	13.1	18.1	21.1	20.1	18.4	13.2	15.9
Tall Grass	7.1	13.1	18.2	21.1	20.1	18.4	13.1	15.9
Forest	7.2	13.4	17.9	20.8	19.8	18.2	13.2	15.8
Corn	6.4	12.9	18.0	20.4	19.1	17.3	12.1	15.2
Average daily maximum surface temperature (°C)								
Asphalt	32.6	39.9	47.6	53.2	48.9	40.8	27.5	41.5
Concrete	28.5	35.8	43.0	48.3	44.4	36.9	24.4	37.3
Bare soil	22.0	28.9	35.0	41.0	38.9	32.0	21.3	31.3
Corn	16.6	22.8	26.2	26.7	24.3	20.2	12.8	21.4
Forest	16.5	19.0	21.0	24.7	23.6	20.2	13.6	19.8
Tall Grass	11.5	17.7	22.5	26.4	25.1	21.3	14.1	19.8
Lawn	11.0	17.2	22.0	25.9	24.7	20.9	14.0	19.4
Average daily minimum surface temperature (°C)								
Lawn	5.9	12.0	16.4	19.9	19.0	15.7	9.7	14.1
Tall grass	5.8	12.0	16.4	19.9	18.9	15.5	9.4	14.0
Forest	5.2	12.2	16.3	19.7	18.8	15.7	9.7	13.9
Concrete	4.2	11.2	16.4	20.2	18.5	13.8	6.3	12.9
Bare soil	3.4	10.5	15.5	19.6	18.5	13.7	6.4	12.5
Corn	3.9	10.4	15.2	18.5	17.4	13.7	7.5	12.4
Asphalt	3.1	10.2	15.3	19.0	17.4	12.8	5.4	11.9
Average daily amplitude ((maximum−minimum)/2) surface temperature (°C)								
Asphalt	14.7	14.8	16.1	17.1	15.7	14.0	11.1	14.8
Concrete	12.2	12.3	13.3	14.1	12.9	11.6	9.1	12.2
Bare soil	9.3	9.2	9.7	10.7	10.2	9.1	7.4	9.4
Corn	6.4	6.2	5.5	4.1	3.5	3.3	2.7	4.5
Forest	5.7	3.4	2.3	2.5	2.4	2.3	1.9	2.9
Tall grass	2.8	2.8	3.1	3.3	3.1	2.9	2.3	2.9
Lawn	2.6	2.6	2.8	3.0	2.9	2.6	2.2	2.7

Table 10 Summary of process equations used in this study for different land use and climate conditions (wet or dry)

Process	Equation numbers	Pavement		Bare soil		Vegetated	
		Dry	Wet	Dry	Wet	Dry	Wet
Soil/pavement conduction	2–3	×	×	×	×	×	×
Surface heat transfer	4–12	×	×	×	×		
Conduction to runoff	15		×		×		×
Soil moisture	16–20			×	×	×	×
Surface heat transfer with plant canopy	21–32					×	×

An ''×'' indicates use of an equation set for a particular land use and climate condition.

give very similar surface temperatures, about 10 °C lower than pavement in average temperature and 20 °C lower in average daily maximum temperature. Bare soil gives surface temperatures that lie between those for pavements and plant-covered surfaces. Daily minimum temperatures were relatively similar across the different land uses, with only 3–6 °C separating the highest (concrete) from the lowest (tall grass prairie).

For wet weather conditions, surface temperatures vary much less between land uses (Fig. 12, upper panel and Table 9). Even in July, average wet weather surface temperature varied only from 22.9 °C for concrete to 20.4 °C for corn. For most rainfall events, warmer ground surface such as asphalt cool significantly as cloud cover increases, prior to the onset of rainfall. Average wet weather temperatures peak slightly later in the year, late July, compared to mid-July for all weather temperatures (Fig. 12).

Summary and conclusions

A temperature model has been formulated and applied to simulate ground surface and soil temperatures for a wide range of surface covers from asphalt pavements to forests. The process equations used in this study for differing land use conditions and wet or dry weather are summarized in Table 10. The temperature model includes relationships to calculate dry weather heat fluxes between the atmosphere and the ground surface (solar and atmospheric radiation, evaporation, convection) and conduction from the ground. Under wet weather conditions heat fluxes by precipitation and surface water runoff are added. The thermal properties of a wet surface vs. a dry surface are accounted for. Surface runoff can be an important heat flux component during periods of rainfall. Although the soil heat conduction model used in this study was relatively simple compared to models of Asaeda and Ca (1993) and Sophocleous (1979), it was found to be sufficient for the purposes of this study. The model has the capability of performing continuous simulations of surface temperatures for periods of six months.

Ground surface temperatures were simulated from a balance of the individual heat flux components. Heat fluxes through plant canopies to a ground surface were formulated separately. Continuous time series simulations of ground surface temperatures including dry and wet weather periods, have been made for eight ground covers (asphalt, concrete, bare soil, lawn, tall grass prairie, corn and soy bean crops and forests) by switching to the appropriate heat flux equations when the weather changes from dry to wet. The different ground covers require changes in the specification of thermal properties, e.g. of canopies, and to a minor degree of soils. The simulations are made with the assumption of equilibrium among heat fluxes, with the exception of heat conduction from the soil and infiltration of water into the soil.

The relatively detailed, mechanistic formulation of the surface heat transfer fluxes results in good agreement of simulated and observed values of surface temperatures at short time scales, e.g. 15 min. The soil temperature and moisture model handles bare soil and pavement quite well, with RMSE values of about 2 °C for bare soil and 1 °C for pavement. The higher simulation error of the bare soil is likely due to inaccuracy of the simulated soil moisture content and the resulting error in calculating heat flux by surface evaporation. The plant canopy model provides an adequate approximation for the effect of vegetation on surface heat transfer. It uses only a few additional parameters compared to bare surfaces.

The seasonal variability of mean ground surface temperatures in the temperate region of the US is clearly illustrated in Fig. 12. The differences among the different ground covers that are obvious in the mean surface temperatures are also evident in the daily maximum surface temperatures given in Table 9. As expected, pavements have the highest surface temperatures. Bare soil was found to have surface temperatures lower than those of pavement but higher than those of surfaces with plant covers. Different vegetation types under the same climate conditions gave very similar results for ground surface temperature, particularly for mid-summer, when all plants had nearly full density (surface coverage). Monthly-averaged wet weather ground surface temperatures varied relatively little between land uses (2.5 °C in July) compared to all weather temperatures (10.4 °C in July).

The information on ground surface temperatures is useful to estimate the impact of different ground covers on thermal pollution of coldwater (trout) streams. Coldwater streams are typically fed by groundwater and surface runoff. The water temperature of surface runoff and the temperature of shallow groundwater both depend on the ground surface temperatures. Ground surface temperatures are therefore useful to assess the impact of changes in land use, e.g. by urban development, on coldwater streams and their fish habitat.

Acknowledgments

This study was conducted with support from the Minnesota Pollution Control Agency, St. Paul, Minnesota, with Bruce Wilson as the project officer. Soil temperature and climate data used in this study were acquired from:

(1) Dr. David Ruschy, University of Minnesota, Department of Soil, Climate and Water, St. Paul, MN.
(2) Ben Worel and Tim Clyne, Minnesota Department of Transportation.
(3) The Natural Resources Conservation Service Soil and Climate Analysis Network (http://www.wcc.nrcs.usda.gov/scan).
(4) The Ameriflux web site (http://public.ornl.gov/ameriflux/). The PI responsible for the Bondville measurement site is Tilden Meyers NOAA/ARL, Atmospheric Turbulence and Diffusion Division. The PIs responsible for the Batavia site are Roser Matamala, David Cook, Julie Jastrow, and Barry Lesht (Argonne National Laboratory), Miquel Gonzalez-Meler (University of Illinois at Chicago), and Gabriel Katul (Duke University).

We are grateful to these individuals and organizations for their cooperation.

References

Asaeda, T., Ca, V.T., 1993. The subsurface transport of heat and moisture and its effect on the environment. Boundary-Layer Meteorology 65, 159–179.

Best, M.J., 1998. A model to predict surface temperature. Boundary-Layer Meteorology 88, 279–306.

Best, M.J., Cox, P.M., Warrilow, D., 2005. Determining the optimal soil temperature scheme for atmospheric modeling applications. Boundary-Layer Meteorology 114, 111–142.

Bigl, S.R., Berg, R.L., 1996. Modeling of Mn/ROAD test sections with the CRREL mechanistic pavement design procedure. Special Report 96-21, US Army Corps of Engineers, Cold Regions Research and Engineering Laboratory.

Dang, H., Gillett, N.P., Weaver, A.J., Zwiers, F.W., 2007. Climate change detection over different land surface vegetation classes. International Journal of Climatology 27 (2), 211–220.

Deardorff, J.W., 1978. Efficient prediction of ground surface temperature and moisture with inclusion of a layer of vegetation. Journal of Geophysical Research 83, 1889–1903.

de Vries, D.A., 1958. Simultaneous transfer of heat and moisture in porous media. Transactions – American Geophysical Union 39 (5), 909–915.

Diefenderfer, B.K., Al-Qadi, I.L., Diefenderfer, S.D., 2006. Model to predict pavement temperature profile: development and validation. Journal of Transportation Engineering 132 (2), 162–167.

Eckert, E.R.G., Drake Jr., R.M., 1972. Analysis of Heat and Mass Transfer. McGraw-Hill, New York.

Edinger, J.E., Duttweiler, D.W., Geyer, J.C., 1968. The response of water temperatures to meteorological conditions. Water Resources Research 4 (5), 11145–11337.

Edinger, J.E., Brady, D.K., Geyer, J.C., 1974. Heat exchange in the environment. Report No. 14, Cooling Water Discharge Research Project RP-49, Electric Power Research Institute, Palo Alto, CA, 125 pp.

Emmerich, W.E., Woolhiser, D.A., Shirly, E.D., 1989. Comparison of lumped and distributed models for chemical transport by surface runoff. Journal of Environmental Quality 18, 120–126.

Hermansson, A., 2001. Mathematical model for calculation of pavement temperatures: comparison of calculated and measured temperatures. Transportation Research Record 1764, 180–188.

Kleinman, P.J.A., Srinivasan, M.S., Dell, C.J., Schmidt, J.P., Sharpley, A.N., Bryant, R.B., 2006. Role of rainfall intensity and hydrology in nutrient transport via surface runoff. Journal of Environmental Quality 35, 1248–1259.

Li, R.M., Stevens, M.A., Simons, D.B., 1976. Solutions to Green–Ampt infiltration equation. Journal of irrigation and drainage engineering, ASCE 102 (2), 239–248.

Luo, Y., Loomis, R.S., Hsiao, T.C., 1992. Simulation of soil temperature in crops. Agricultural and Forest Meteorology 61, 23–38.

Mengelkamp, H.T., Warrach, K., Rascke, E., 1999. SEWAB – a parameterization of the surface energy and water balance for atmospheric and hydrologic models. Advances in Water Resources 23, 165–175.

Mihailovic, D.T., Eitzinger, J., 2007. Modelling temperatures of crop environment. Ecological Modelling 202, 465–475.

Patankar, S.V., 1980. Numerical Heat Transfer and Fluid Flow. McGraw-Hill, New York.

Roa-Espinosa, A., Norman, J.M., Wilson, T.B., Johnson, K., 2003. Predicting the impact of urban development on stream temperature using a thermal urban runoff model (TURM). In: Proceedings, US EPA National Conference on Urban Stormwater: Enhancing Programs at the Local Level, February 17–20, Chicago, IL, pp. 369–389.

Ryan, P.J., Harleman, D.R.F., Stolzenbach, K.D., 1974. Surface heat loss from cooling ponds. Water Resources Research 10 (5), 930–938.

Sophocleous, M., 1979. Analysis of water and heat flow in unsaturated–saturated porous media. Water Resources Research 15 (5), 1195–1206.

Ul Haq, R., James, W., 2002. Thermal enrichment of stream temperature by urban storm water. In: Proceedings, International Conference on Urban Drainage, Portland, OR.

Van Buren, M.A., Watt, W.E., Marsalek, J., Anderson, B.C., 2000. Thermal enhancement of stormwater runoff by paved surfaces. Water Resources 34 (4), 1359–1371.